Servo-Integrated Patterned Media by Hybrid Directed Self-Assembly

Shuaigang Xiao,* Xiaomin Yang, Philip Steiner, Yautzong Hsu, Kim Lee, Koichi Wago, and David Kuo

Media Research Center, Seagate Technology, 47010 Kato Road, Fremont, California 94538, United States

ABSTRACT A hybrid directed self-assembly approach is developed to fabricate unprecedented servo-integrated bit-patterned media templates, by combining sphere-forming block copolymers with 5 teradot/in.^{2} resolution capability, nanoimprint and optical lithography with overlay control. Nanoimprint generates prepatterns with different dimensions in the data field and servo field, respectively, and optical lithography controls the selective self-assembly process in either field. Two distinct directed self-assembly techniques, low-topography graphoepitaxy and high-topography graphoepitaxy, are elegantly integrated to create bit-patterned templates with flexible embedded servo information. Spinstand magnetic test at 1 teradot/in.^{2} shows a low bit error rate of $10^{-2.43}$, indicating fully functioning bit-patterned media and great potential of this approach for fabricating future ultra-high-density magnetic storage media.

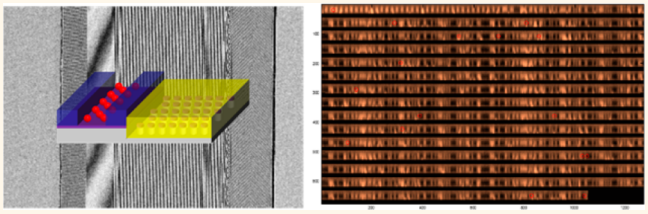

KEYWORDS: block copolymer · directed self-assembly · overlay · servo integration · spinstand · bit-patterned media

In response to the continuing digital data explosion, data storage media with ultrahigh density and low cost are yearned for by enormous data centers nowadays. As a major supplier of storage solutions, the hard disk drive industry is heavily investing in several next-generation magnetic recording technologies beyond conventional perpendicular magnetic recording (PMR), such as heat-assisted magnetic recording (HAMR)[1] and bit-patterned media (BPM).[2] Both HAMR and BPM help retard the appearance of an ultimate physic limit called the superparamagnetic limit,[3] relying on the improvement of the recording media's thermal stability *via* increasing either the anisotropy field or the effective volume of each magnetic grain. The first hurdle of obtaining high-density BPM is the generation of a master nanoimprint template, called a BPM template in this paper, *via* lithography for high-volume manufacturing of bit-patterned disks. The BPM template needs to start with a pattern density of 1 teradot/in.^{2} (Tdpsi), at least, so as to be competitive with PMR or HAMR, which is not trivial for the current nanolithography society.

Directed self-assembly (DSA), based on block copolymer materials, is deemed as one of the alternative nanolithography techniques for potential applications in nanoelectronics,[4,5] nanophotonics,[6] nanosensors,[7] and nanofluidics.[8] In DSA, the combination of a high-χ (χ is the Flory–Huggins interaction parameter) block copolymer and commensurate prepatterns ensures both high resolution and good addressability, which is critical for applications with stringent requirements on pattern uniformity and feature placement accuracy, such as BPM. Depending on the driving force, DSA has been typically divided into three categories: chemoepitaxy,[9−11] high-topography graphoepitaxy (HTG),[12−15] and low-topography graphoepitaxy (LTG).[16−18] Chemoepitaxy is based on a prepattern with mainly high chemical contrast plus low topography contrast; that is, the topography or feature height in the prepattern $h \ll L_0$, where L_0 is the natural domain spacing of the block copolymer. HTG, which is usually called graphoepitaxy, relies on a prepattern with mainly high topography contrast; that is, h is comparable to or larger than L_0. In addition, LTG employs a prepattern with negligible chemical contrast and low topography contrast, *i.e.*, $h \ll L_0$. As an example, we reported a route using nanoimprint lithography (NIL) to create commensurate resist prepatterns for both HTG and LTG of sphere-forming polystyrene-*block*-polydimethylsiloxane (PS-*b*-PDMS).[19]

* Address correspondence to shuaigang.xiao@seagate.com.

Received for review October 2, 2014 and accepted November 7, 2014.

Published online November 07, 2014
10.1021/nn505630t

So far, there have been a few research groups exploring DSA for BPM template application, including ourselves.[20−24] An ideal BPM template should include both data field and servo field. The data field consists of globally close packed periodic dots with tight size and position sigma control. In comparison, in one kind of BPM servo called an embedded servo,[25] the servo field consists of patterned alternating thermally stable magnetic areas and nonmagnetic areas. A Si template with an embedded servo was generated *via* HTG in both the data field and servo field previously.[20] However, drawbacks of that approach include significant loss of real estate and poor control of dot pattern quality in the data field, due to the high topography in the prepatterns. An idea to create flexible two-dimensional (2-D) dot arrays is to overlap two DSA line patterns at an orthogonal or oblique angle *via* chemoepitaxy,[21,22] which smartly resolves the limit of the skew angle[23] in the BPM design. But a solution to incorporate complex and flexible servo information into such a dot patterning process is still not clear. Here, a hybrid DSA route is developed to meet the challenge of servo integration while ensuring high-quality dot patterning in the data field. BPM templates with an embedded servo are thus fabricated, and bit error rate (BER) demonstration on a spinstand tester succeeds for the first time.

RESULTS AND DISCUSSION

Hybrid DSA with Overlay Control to Fabricate Servo-Integrated BPM Templates. A process-friendly servo design is critical for servo integration. The servo selected here is called an embedded servo, which exists in each track among data sectors and serves for write synchronization and track-following purposes.[25] Ideally the data field has 100% pattern occupancy to maximize bit areal density across the whole disk surface, and the servo field requires only ~50% pattern occupancy to provide alternate ON/OFF signals. To fulfill the 100% pattern occupancy goal in the data field, either chemoepitaxy or LTG is preferred to deliver globally close-packed dot arrays with tight dot size and position sigma control. Another advantage in both cases is that the prepattern with low topography has little effect on latter pattern transfer since it is buried under the resulting DSA pattern. As for the servo field, HTG gives the best tolerance of variable servo patterns, such as phase lock loop (PLL), address mark, gray code, and position error signal (PES),[25] by generating patches of locally close-packed dot arrays with short-range order separated by an unpatterned area. As demonstrated recently, NIL is able to create resist prepatterns with adjustable topography for both HTG and LTG of sphere-forming PS-*b*-PDMS.[19] So it is selected as the way to produce resist prepatterns with various feature dimensions in the data field and servo field simultaneously on a substrate. As shown in Figure 1A, the data prepattern

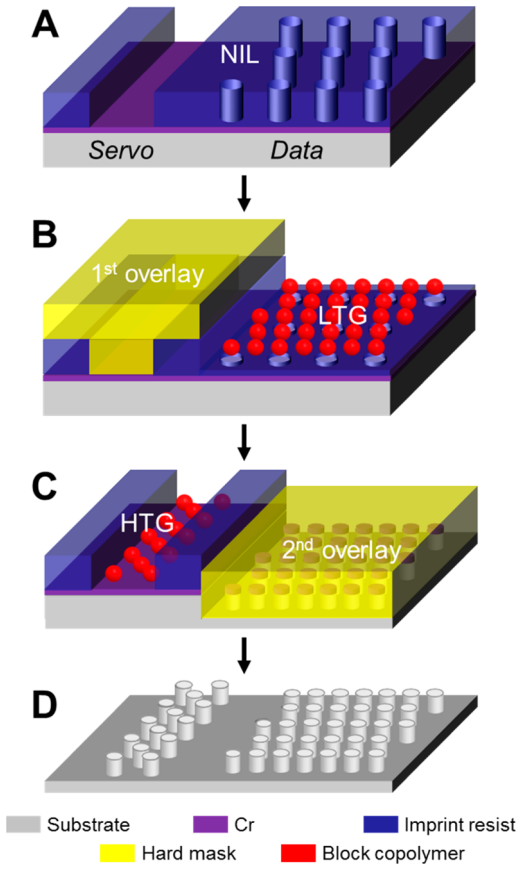

Figure 1. Hybrid DSA with overlay control to fabricate a servo-integrated BPM template, by combining DSA, NIL, and optical lithography. (A) Prepatterns in both the data field and servo field defined by NIL. (B) First overlay to protect the servo field, followed by resist thinning and LTG in the data field. (C) Pattern transfer in the data field and second overlay to protect the data field, followed by HTG in the servo field. (D) BPM template with embedded servo.

consists of low-density 2-D hole arrays with critical dimensions (CDs) and hole depths comparable to L_0. In comparison, the servo prepatterns consist of 1-D or quasi 1-D trench patterns with CDs of 3−10 L_0 and the same depths. The concept of overlay control by optical lithography is introduced then for selective DSA in either the data field or servo field, since uniform DSA patterns in both the data field and servo field are difficult to obtain in a single DSA step due to different DSAs (*i.e.*, LTG *vs* HTG) requiring different initial block copolymer film thicknesses. As an example shown in Figure 1B, an optical lithography step with overlay control, denoted as the first overlay, is performed to protect the servo field with a hard mask layer. By using an oxygen plasma process, the topography of the data prepattern is reduced to a few nanometers. The resulting low-topography 2-D prepattern with $h \ll L_0$ is used for LTG in the data field. After pattern transfer, another optical lithography step also with overlay control, denoted as the second overlay, is executed to protect the data field at this time (Figure 1C). The high-topography1-D prepattern with $h \approx L_0$ is used for

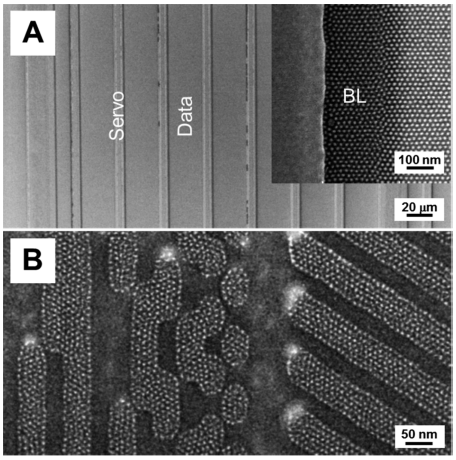

Figure 2. Distinct DSA behavior of sphere-forming PS-*b*-PDMS in the data field and servo field, respectively. (A) LTG of 2 Tdpsi PS-*b*-PDMS dots with L_N = 38.3 nm and L_0 = 19.2 nm in the data field (majority area) *via* thermal annealing. The inset shows a narrow BL region around an optical lithography boundary. (B) HTG of 5 Tdpsi PS-*b*-PDMS dots with L_0 = 12.2 nm in the servo field *via* solvent annealing.

HTG in the servo field. Finally, after pattern transfer in the servo field and removal of the residual hard mask and polymer, a servo-integrated BPM template is formed, consisting of globally close-packed dot arrays in the data field and locally close-packed dot arrays in the servo field (Figure 1D). Overall, decoupling of DSA in the data field and DSA in the servo field makes it possible for various high-density dot arrays to be achieved on the same substrate without sacrificing either pattern occupancy or pattern uniformity. Overlay control during optical lithography plays an important role here to guarantee selective DSA in the selected field.

Distinct DSA Behavior in the Data Field and Servo Field up to 5 Tdpsi. On a substrate that has been run through first overlay, there exists a series of topography changes with a step height Δh that is on the order of tens of nanometers and comes from the imprint resist layer and the hard mask layer, at the optical lithography boundary of each opened data field. Although LTG of sphere-forming PS-*b*-PDMS on an almost flat substrate has been proved before,[16,19] DSA pattern uniformity over a substrate with large topography change still needs investigation. As shown in Figure 2A, the opened data field occupies the majority of the area, with the servo field coexisting in between. After spin-coating of block copolymer solutions, block copolymer thin films look uniform all over the data field in the form of monolayered PDMS spheres surrounded by a PS matrix, with a pattern density of 2 Tdpsi. The inset shows DSA behavior around an optical lithography boundary with Δh = 46 nm. DSA of most block copolymer dots behaves as LTG in response to an underlying low-topography 2-D resist prepattern with L_N = 38.3 nm, where L_N is the pattern pitch defined by NIL. There exist 1 or 2 rows of block copolymer dots

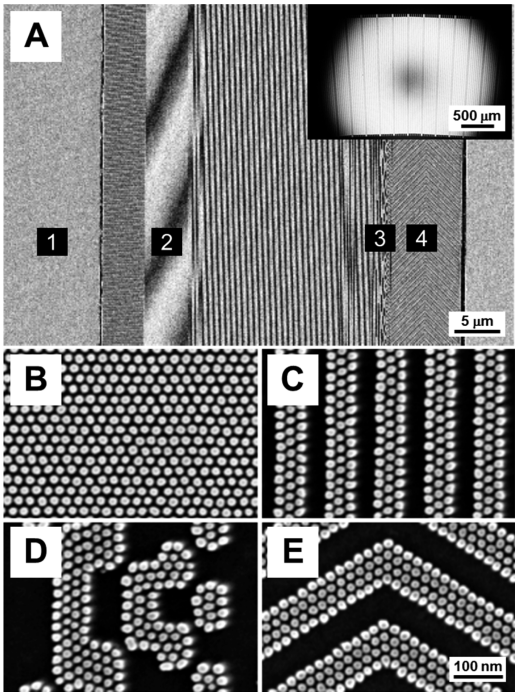

Figure 3. Servo-integrated BPM template at 1 Tdpsi. (A) Moiré pattern of a servo sector between two data sectors. The inset shows multiple data/servo sectors. Labels 1−4 indicate data pattern labeled as 1 (B), PLL pattern labeled as 2 (C), gray code pattern labeled as 3 (D), and PES pattern labeled as 4 (E).

aligned along the sidewall according to the mechanism of HTG. Besides, there is also a narrow bilayer (BL) region having a local film thickness increase from L_0 (=19.2 nm) to $\sim 2L_0$ (close to Δh) due to the wall effect. The width of the BL region can be decreased significantly when Δh is decreased toward L_0 (not shown). Nonetheless, DSA patterns are quite uniform in a monolayer form over 98−99% area of the data field.

Usually, thermaling anneal is sufficient to drive PS-*b*-PDMS molecules in thin films from micelle structures to ordered nanostructures such as hexagonal close packed spheres in the form of a monolayer, at a pattern density up to 3.8 Tdpsi.[16] But when a higher pattern density such as 5 Tdpsi is pursued using this material, thermal fluctuations prevent the formation of ordered block copolymer nanodomains with reasonable local-range order. An *N*-methyl-2-pyrrolidone solvent annealing process is more effective to promote long-range ordering of 5 Tdpsi PS-*b*-PDMS on a flat surface.[26] So we applied solvent annealing for HTG of a 5 Tdpsi PS-*b*-PDMS (L_0 = 12.2 nm) in the servo field here. The results are shown in Figure 2B. Locally close packed DSA dots filled up all kinds of servo patterns. Good local-range order was observed, which implies the compatibility of HTG for embedded servo patterns in the ultra-high-density regime.

Servo-Integrated BPM Templates at 1 Tdpsi and Beyond. Figure 3A shows moiré patterns captured around a servo sector on a 1 Tdpsi (L_0 = 27 nm) servo-integrated

BPM template. Each moiré pattern represents either a data pattern or a kind of servo pattern. Several typical patterns are labeled by numbers 1−4, and a portion of the template containing multiple data/servo sectors is revealed in the inset. The data pattern (Figure 3B) consists of hexagonal close packed dots with global long-range order, which is fabricated *via* LTG using a 2-D prepattern with L_N = 54 nm and $h \ll L_0$. Addressability of every dot is critical to ensure latter write synchronization and track following after media fabrication and during read/write operation. So both dot size uniformity and dot placement accuracy need to be under control. In comparison, the servo patterns shown in Figure 3C−E, PLL/gray code/PES, consist of close packed dots with local-range order, which are generated *via* HTG using 1-D or quasi 1-D prepatterns with $h \approx L_0$. Addressability of each single dot is not strictly required in this case as long as every dot is magnetically stable after pattern transfer from the template into media. Assembly behavior of each servo pattern is more important for the performance of the whole servo sector in this case. Overall, our unique strategy of 2-D LTG in the data field and 1-D HTG in the servo field executed separately ensures both addressability in the data field and flexibility in the servo field.

As sphere-forming PS-*b*-PDMS is adopted to form DSA patterns in both the data field and servo field in our method, high-fidelity pattern transfer needs to be demonstrated since the feature aspect ratio of spheres is relatively low compared to that of perpendicularly oriented cylinders or lamellae from block copolymers. Pattern transfer results of 2 Tdpsi PS-*b*-PDMS are shown in Figure S1. Whether in the servo field (gray code as shown) or in the data field, dot pattern quality is maintained after pattern transfer from block copolymer spheres to quartz nanopillars in a BPM template with a pillar height of 20 nm. Analyses of both dot size and dot spacing sigmas are shown in Table S1. Although the dot diameter on average increases, the sigma values (1σ/mean) are almost kept constant after pattern transfer, *i.e.*, ∼5−6%, which is impressive in consideration of the pattern density, 2 Tdpsi, discussed here.

Spinstand Test of 1 Tdpsi BPM to Demonstrate a BER of $10^{-2.43}$. After making a servo-integrated template, the next step is to fabricate BPM on a disk. A process called tone-reversal is applied to transfer all the pattern information from the template to a magnetic media.[24] As for characterization methodology of a BPM disk, not only is an optical surface analyzer or a scanning electron microscope used for physical visualization, but also a magnetic tester is needed for BER demonstration. Without an integrated servo, only an incomplete BER characterization can be done on a static tester.[27] Here, owing to the incorporation of an embedded servo, a complete full-track BER demonstration at 1 Tdpsi was performed using a spinstand tester,

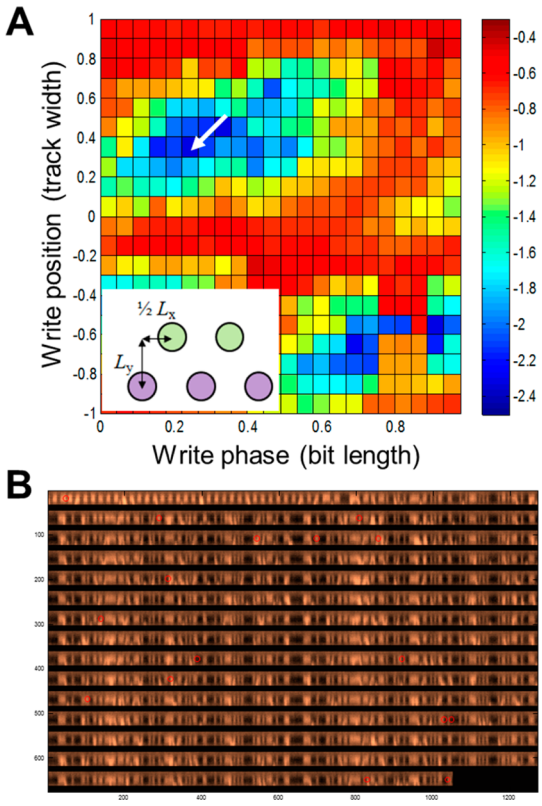

Figure 4. Spinstand test of 1 Tdpsi BPM media with embedded servo. (A) 2-D BER contour as a function of write phase (*x*-axis) in units of bit length L_x and write position (*y*-axis) in units of track width L_y. The arrow indicates an optimal point with the best BER. The inset illustrates two adjacent dot rows with (1/2)L_x placement shift in the *x*-direction and L_y placement shift in the *y*-direction. (B) Read-back signals of a PRBS starting from the middle of the topmost row, at the above optimal point. The red circles show the locations of bit errors.

which is the first time that BPM were fabricated by DSA. Figure 4A shows a 2-D BER contour map as a function of write phase (*x*-axis or down-track direction) and write position (*y*-axis or cross-track direction). There exist two sweat regions with low BER values on the map, one located at the upper-left blue portion and the other located at the lower-right blue portion. Write phase shift between those two regions is about one-half of the bit length L_x, where L_x is equal to L_0, and write position shift is about one track width L_y, where L_y is equal to 0.866L_0 in a hexagon lattice. Those two sweat regions correspond to two adjacent dot rows which deviate from each other by (1/2)L_x in the *x*-direction and L_y in the *y*-direction, as shown in the inset. The optimal BER data point, $10^{-2.43}$, is indicated by an arrow. Detailed read-back signals at this optimal BER point are revealed in Figure 4B. To obtain convincing statistics, more than 4000 dots in a row are selected and written with a predefined pseudorandom bit sequence (PRBS) using a spinstand write head. Then the PRBS signals are read back by a spinstand read head. Bit errors in read-back signals are circled in red. By this means, a 2-D BER contour map as shown in

Figure 4A was reconstructed after collecting read-back signals and analyzing corresponding BERs at hundreds of test conditions of different write phases and write positions.

CONCLUSIONS

A hybrid DSA approach to servo-integrated BPM templates is explored, by combining three lithography techniques: NIL, optical lithography, and DSA. NIL is used to generate prepatterns with different dimensions in the data field and servo field on a substrate. Optical lithography with overlay control is applied to selectively open either the data field or servo field for following DSA processes. 1-D HTG is adopted to accommodate variable pattern designs in the servo field, and 2-D LTG is developed to obtain addressable and uniform nanodot arrays in the data field, separately. DSA patterns of sphere-forming PS-*b*-PDMS up to 5 Tdpsi and high-fidelity pattern transfer results at 2 Tdpsi indicate great potential for ultra-high-density BPM fabrication. Finally, it is the first time that a spin-stand test is realized for BPM fabricated by DSA. A BER of $10^{-2.43}$ obtained at 1 Tdpsi represents great functionality of integrated servo patterns and high-quality data patterns in bit-patterned templates and magnetic storage media.

EXPERIMENTAL SECTION

Materials. Block copolymers and homopolymers were purchased from Polymer Source, Inc. Sphere-forming polystyrene-*block*-polymethylsiloxane (PS-*b*-PDMS) at 1 teradot/in.^{2} (Tdpsi): number-average molecular weight M_n = 22.5k-*b*-4.5k, polydispersity PDI = 1.09, and natural domain spacing L_0 = 27 nm. Sphere-forming PS-*b*-PDMS at 2 Tdpsi: M_n = 11.7k-*b*-2.9k, PDI = 1.09, blended with PS homopolymer, and L_0 = 19.2 nm. Sphere-forming PS-*b*-PDMS at 5 Tdpsi: M_n = 7k-*b*-1.5k, PDI = 1.05, blended with PS homopolymer, and L_0 = 12.2 nm. PS homopolymer: M_n = 3.7 kg/mol, PDI = 1.09. Hydroxyl-terminated PS brush: M_n = 3.2 kg/mol, PDI = 1.1. Imprint resist materials were purchased from Molecular Imprints, Inc. Optical resist materials were purchased from AZ Electronic Materials.

NIL and Optical Lithography. Low-density quartz imprint molds were fabricated with various pattern layouts and pattern densities, by using a rotary-stage electron-beam system. The pillar height of imprint molds is 40 nm. An acrylate-based imprint resist was used as received from Molecular Imprints Inc. After drop-dispensing of UV imprint resist percursors on a 6 in. quartz wafer, the imprint mold was applied to create low-density hole-tone prepatterns in the data field and various trench prepatterns in the servo field, in a 35 nm thick imprint resist layer *via* UV curing. A metallic hard mask layer was deposited on the imprint resist layer, and then a thick I-line resist layer was spin-coated on the hard mask layer, for 365 nm exposure using a Suss MicroTec MA6 contact aligner to selectively open the multi-sector data field or servo field with an overlay accuracy of 0.5 μm or so. Predefined marks on the substrate are used for alignment purposes to give overlay control during the optical lithography step.

1-D High-Topography Graphoepitaxy in the Servo Field. After an optical step to open the servo field, the hard mask in the opened areas was removed by either a dry plasma etch process or a wet chemical etch process. Then PS-*b*-PDMS block copolymer solutions were spin-coated onto the imprint resist film prepatterned with 1-D or quasi 1-D high-topography prepatterns. Directed self-assembly happened during either thermal annealing at 170 °C for 12 h or solvent annealing in an *N*-methyl-2-pyrrolidone vapor atmosphere for 1 h. CF_4 reactive-ion etching (RIE) was applied to remove a thin layer of PDMS on the top surface prior to O_2 RIE for removing unprotected PS blocks so as to reveal oxidized PDMS spheres.

2-D Low-Topography Graphoepitaxy in the Data Field. After an optical step to open the data field, the hard mask in opened areas was removed by either a dry plasma etch process or a wet chemical etch process. O_2 RIE was performed to reduce the thickness of the imprint resist layer down to 5 nm or less. A hydroxyl-terminated PS brush was thermally grafted on the exposed substrate area (with a Cr cover) to provide a uniform wetting condition for PS blocks in the copolymer, together with the remaining imprint resist matrix. Then PS-*b*-PDMS block copolymer solutions were spin-coated onto the imprint resist film prepatterned with 2-D low-topography prepatterns. DSA happened during thermal annealing at 170 °C for 12 h. CF_4 RIE was applied to remove a thin layer of PDMS on the top surface prior to O_2 RIE for removing unprotected PS blocks so as to reveal oxidized PDMS spheres.

Pattern Transfer. Prior to nanoimprinting, a thin layer of Cr (shown in Figure 1) was deposited on the quartz substrate, acting as an intermediate layer for pattern transfer from PS-*b*-PDMS spheres to the substrate, *i.e.*, Cl_2/O_2 RIE from PS-*b*-PDMS to Cr and CF_4 RIE from Cr to quartz. Cl_2/O_2 RIE for Cr etch, O_2 RIE for resist thinning, and CF_4 RIE for quartz substrate etch were performed on plasma etchers made by Oxford Instruments. Cl_2/O_2 RIE experiments were done at 10 mTorr and 100 W. O_2 RIE experiments were done at 10 mTorr and 40 W. CF_4 RIE experiments were done at 2 mTorr and 40 W. Ion-beam etching of magnetic materials was performed on a Veeco argon ion miller.

Characterization and Image Analysis. Imprint resist patterns, DSA patterns, and quartz dot patterns were characterized by using a scanning electron microscope (SEM) operated at 10 keV with a Raith150-Two system from Raith GmbH and an atomic force microscope from Veeco Instruments. DSA patterns were imaged after CF4 + O_2 RIE as described before. Cr of 3 nm thick was deposited onto quartz samples to minimize SEM charging effects. The read-back and recording performance of 1 Tdpsi bit-patterned media was evaluated using an in-house spinstand tester with a commercially available perpendicular magnetic recording head. As for image analysis, the dot was defined as a circle, either inscribed within the dot or circumscribed around the dot's external contour. The dot size was defined as the dot diameter. The dot spacing was defined as the center-to-center distance between two neighboring dots in the *x*-direction. The distribution was defined as a quotient of the standard deviation divided by the mean. Each image includes about 1000 dots for a total of at least 5 images analyzed per pattern. The resolution was chosen so that each dot has ~250 pixels.

Conflict of Interest: The authors declare no competing financial interest.

Acknowledgment. The authors thank H. Yang, M. Feldbaum, Z. Yu, H. Wang, J. Hwu, N. Kurataka, G. Gauzner, and W. Gu for insightful discussions and technical assistance.

Supporting Information Available: Figure S1 and Table S1. This material is available free of charge *via* the Internet at http://pubs.acs.org.

REFERENCES AND NOTES

1. Challener, W. A.; Peng, C.; Itagi, A. V.; Karns, D.; Peng, W.; Peng, Y.; Yang, X.; Zhu, X.; Gokemeijer, N. J.; Hsia, Y.-T.; *et al.* Heat-Assisted Magnetic Recording by a Near-Field Transducer with Efficient Optical Energy Transfer. *Nat. Photonics* **2006**, *3*, 220–224.

2. Ross, C. A. Patterned Magnetic Recording Media. *Annu. Rev. Mater. Res.* **2001**, *31*, 203–235.
3. Weller, D.; Moser, A. Thermal Effect Limits in Ultrahigh-Density Magnetic Recording. *IEEE Trans. Magn.* **1999**, *35*, 4423–4439.
4. Herr, D. J. C. Directed Block Copolymer Self-Assembly for Nanoelectronics Fabrication. *J. Mater. Res.* **2011**, *26*, 122–139.
5. Black, C. T.; Ruiz, R.; Breyta, G.; Cheng, J. Y.; Colburn, M. E.; Guarini, K. W.; Kim, H.-C.; Zhang, Y. Polymer Self Assembly in Semiconductor Microelectronics. *IBM J. Res. Dev.* **2007**, *51*, 605–633.
6. Walavalkar, S. S.; Hofmann, C. E.; Homyk, A. P.; Henry, M. D.; Atwater, H. A.; Scherer, A. Tunable Visible and Near-IR Emission from Sub-10 nm Etched Single-Crystal Si Nanopillars. *Nano Lett.* **2010**, *10*, 4423–4428.
7. Wells, S. M.; Merkulov, I. A.; Kravchenko, I. I.; Lavrik, N. V.; Sepaniak, M. J. Silicon Nanopillars for Field-Enhanced Surface Spectroscopy. *ACS Nano* **2013**, *6*, 2948–2959.
8. Cheng, L.; Cao, D. Designing a Thermo-Switchable Channel for Nanofluidic Controllable Transportation. *ACS Nano* **2011**, *5*, 1102–1108.
9. Kim, S. O.; Solak, H. H.; Stoykovich, M. P.; Ferrier, N. J.; de Pablo, J. J.; Nealey, P. F. Epitaxial Self-Assembly of Block Copolymers on Lithographically Defined Nanopatterned Substrates. *Nature* **2003**, *424*, 411–414.
10. Cheng, J. Y.; Rettner, C. T.; Sanders, D. P.; Kim, H. C.; Hinsberg, W. D. Dense Self-Assembly on Sparse Chemical Patterns: Rectifying and Multiplying Lithographic Patterns using Block Copolymers. *Adv. Mater.* **2008**, *20*, 3155–3158.
11. Ruiz, R.; Kang, H. M.; Detcheverry, F. A.; Dobisz, E.; Kercher, D. S.; Albrecht, T. R.; de Pablo, J. J.; Nealey, P. F. Density Multiplication and Improved Lithography by Directed Block Copolymer Assembly. *Science* **2008**, *321*, 936–939.
12. Segalman, R. A.; Yokoyama, H.; Kramer, E. J. Graphoepitaxy of Spherical Domain Block Copolymer Films. *Adv. Mater.* **2001**, *13*, 1152–1155.
13. Sundrani, D.; Darling, S. B.; Sibener, S. J. Guiding Polymers to Perfection: Macroscopic Alignment of Nanoscale Domains. *Nano Lett.* **2004**, *4*, 273–276.
14. Cheng, J. Y.; Mayes, A. M.; Ross, C. A. Nanostructure Engineering by Template Self-Assembly of Block Copolymers. *Nat. Mater.* **2004**, *3*, 823–828.
15. Bita, I.; Yang, J. K. W.; Jung, Y. S.; Ross, C. A.; Thomas, E. L.; Berggren, K. K. Graphoepitaxy of Self-Assembled Block Copolymers on Two-Dimensional Periodic Patterned Templates. *Science* **2008**, *321*, 939–943.
16. Xiao, S.; Yang, X.; Park, S.; Weller, D.; Russell, T. P. A Novel Approach to Addressable 4 Teradot/in^2 Patterned Media. *Adv. Mater.* **2009**, *21*, 2516–2519.
17. Park, S.; Lee, D. H.; Xu, J.; Kim, B.; Hong, S. W.; Jeong, U.; Xu, T.; Russell, T. P. Macroscopic 10-Terrabit-per-Square-Inch Arrays from Block Copolymers with Lateral Order. *Science* **2009**, *323*, 1030–1033.
18. Hong, S. W.; Gu, X.; Huh, J.; Xiao, S.; Russell, T. P. Circular Nanopatterns over Large Areas from The Self-Assembly of Block Copolymers Guided by Shallow Trenches. *ACS Nano* **2011**, *5*, 2855–2860.
19. Xiao, S.; Yang, X.; Hwu, J. J.; Lee, K. Y.; Kuo, D. A Facile Route to Regular and Nonregular Dot Arrays by Integrating Nanoimprint Lithography with Sphere-Forming Block Copolymer Directed Self-Assembly. *J. Polym. Sci., Polym. Phys.* **2014**, *52*, 361–367.
20. Yamamoto, R.; Yuzawa, A.; Shimada, T.; Ootera, Y.; Kamata, Y.; Kihara, N.; Kikitsu, A. Nanoimprint Mold for 2.5 Tbit/in.^{2} Directed Self-Assembly Bit Patterned Media with Phase Servo Pattern. *Jpn. J. Appl. Phys.* **2012**, *51*, 046503.
21. Ruiz, R.; Dobisz, E.; Albrecht, T. R. Rectangular Patterns Using Block Copolymer Directed Assembly for High Bit Aspect Ratio Patterned Media. *ACS Nano* **2011**, *5*, 79–84.
22. Wan, L.; Ruiz, R.; Gao, H.; Patel, K. C.; Lille, J.; Zeltzer, G.; Dobisz, E. A.; Bogdanov, A.; Nealey, P. F.; Albrecht, T. R. Fabrication of Templates with Rectangular Bits on Circular Tracks by Combining Block Copolymer Directed Self-Assembly and Nanoimprint Lithography. *J. Micro/Nanolith. MEMS MOEMS* **2012**, *11*, 031405.
23. Xiao, S.; Yang, X.; Lee, K. Y.; Veerdonk, R. J. M. v. d.; Kuo, D.; Russell, T. P. Aligned Nanowires and Nanodots by Directed Block Copolymer Assembly. *Nanotechnology* **2011**, *22*, 305302–305309.
24. Xiao, S.; Yang, X.; Lee, K. Y.; Hwu, J. J.; Wago, K.; Kuo, D. Directed Self-Assembly for High-Density Bit-Patterned Media Fabrication Using Spherical Block Copolymers. *J. Micro/Nanolith. MEMS MOEMS* **2013**, *12*, 031110.
25. Ashar, K. G. *Magnetic Disk Drive Technology*; IEEE Press: Piscataway, NJ, 1997.
26. Gu, W.; Xu, J.; Kim, J.-K.; Hong, S. W.; Wei, X.; Yang, X.; Lee, K. Y.; Kuo, D. S.; Xiao, S.; Russell1, T. P. Solvent-Assisted Directed Self-Assembly of Spherical Microdomain Block Copolymers to High Areal Density Arrays. *Adv. Mater.* **2013**, *25*, 3677–3682.
27. Albrecht, T. R.; Bedau, D.; Dobisz, E.; Gao, H.; Grobis, M.; Hellwig, O.; Kercher, D.; Lille, J.; Marinero, E.; Patel, K.; Ruiz, R.; Schabes, M. E.; Wan, L.; Weller, D.; Wu, T.-W. Bit Patterned Media at 1 Tdot/in^2 and Beyond. *IEEE Trans. Magn.* **2013**, *49*, 773–778.